International Journal of Modern Physics E
Vol. 15, No. 7 (2006) 1495–1503

World Scientific
www.worldscientific.com

SHELL STRUCTURE, COLLECTIVITY AND NUCLEAR SHAPES — RISING IN-BEAM EXPERIMENTS AT RELATIVISTIC ENERGIES

PIETER DOORNENBAL for the RISING Collaboration

Institut für Kernphysik, Universität zu Köln,
Zülpicher Straße 77, Köln, 50937, Germany
p.doornenbal@gsi.de

Received 1 October 2006

The RISING fast beam campaign aims at high resolution γ-ray spectroscopy experiments with relativistic radioactive beams at GSI. The secondary beams produced by fragmentation or fission are used for Coulomb excitation or secondary fragmentation experiments to perform studies of nuclei far off stability. The physics phenomena studied with this method include nuclear structure experiments targeting at the evolution of shell structure toward the drip lines, mirror symmetry, collectivity and electromagnetic transition strengths. Example results of this fast beam campaign are presented and compared to various shell model calculations and nuclear structure models.

1. Introduction

The RISING (Rare ISotope INvestigations at GSI) setup for in-beam experiments at relativistic energies consists of the fragment separator FRS and a highly efficient γ-detector array at the final focus of the FRS, composed of EUROBALL Ge-Cluster detectors, MINIBALL Ge-detectors and BaF_2 detectors from the HECTOR array.[1–4] The investigated nuclei are produced via fragmentation reactions or fission of relativistic heavy ions. In the in-beam campaign fast beams in the range of 100 to 300 $A \cdot$ MeV were used for Coulomb Excitation and two-step fragmentation experiments.

The following topics were covered in the nuclear structure experiments performed within the RISING fast beam campaign:

(i) shell structure and its modifications in nuclei far off stability,
(ii) isospin symmetry along the $N = Z$ line,
(iii) shapes and shape coexistence,
(iv) collective modes and $E1$ strength distributions.

1.1. *Monopole driven shell structure*

The monopole part of the residual interaction controls the propagation of single particle energies with increasing occupation of a major shell.[5] It causes the change in shell structure for very neutron-rich nuclei along the $N = 8, 20$ and 28 isotonic sequences, which is due to the $(\sigma\sigma)(\tau\tau)$ term of the residual interaction, where σ and τ indicate the spin and isospin operators. This term is strongly binding for proton-neutron, spin-flip and spin-orbit partners and leads to a change of harmonic oscillator shell closures with magic numbers $N_m = 8, 20$ to $N_m - 2 \times N = 6, 16(14)$, N being the harmonic oscillator main quantum number.[6,7] For the weak $N = 40$ harmonic oscillator case it should find its continuation in a $N = 32, 34$ subshell closure.[7] The monopole driven shell evolution far off stability is expected to be of isospin symmetric nature, which may be studied in $N = 20$ isotones and their $Z = 20$ mirror nuclei.

The RISING experiment gives access to excitation energies $E_{2_1^+}$ of $I^\pi = 2_1^+$ states and $B(E2; 2_1^+ \rightarrow 0^+)$ values and can be used as signatures for shell structure. Two type of experiments were performed: First, a Coulomb excitation experiment of the neutron rich ^{54,56,58}Cr, which are located at a key point on the pathway from the $N = 40$ subshell closure across a deformed region to spherical nuclei at $N = 28$, second, a two step fragmentation experiment to investigate the mirror energy difference, defined as $\Delta E_M = E_x(I, T_z = -T) - E_x(I, T_z = +T)$, between ^{36}Ca and ^{36}S.

1.2. *Deformed nuclear shapes between closed shells*

The $A \approx 130$ region shows evidence of stable triaxial shapes.[8] There are also some indications in this transitional region for chiral doublet structures in odd-odd $N = 75$ isotones.[9] The $N = 74$ even-even nuclei ^{132}Ba, ^{134}Ce and ^{136}Nd are the core nuclei of ^{132}La, ^{134}Pr and ^{136}Pm and therefore the collective properties of these nuclei are of great interest and good candidates to search for signs of triaxial deformation. Relativistic Coulomb excitation experiments where performed in ^{134}Ce and ^{136}Nd.

2. Experimental Details

The SIS facility at GSI provides primary beams of all stable nuclei up to ^{238}U with a projectile energy up to 1 $A \cdot$ GeV and intensities up to 10^9/s are available. These beams are incident upon a ^{9}Be target at the entrance of the FRS. The fragments of interest are selected with the Bρ-ΔE-Bρ method by placing a wedge-shaped aluminum degrader at the middle focal plane of the FRS, optimizing the secondary beam at the final focus. The particles are identified in-flight on an event-by-event basis using their magnetic rigidity Bρ, their time of flight between the two scintillation detectors SCI1 and SCI2, see Fig. 1, and their energy loss in the multi sampling ionization chamber MUSIC.

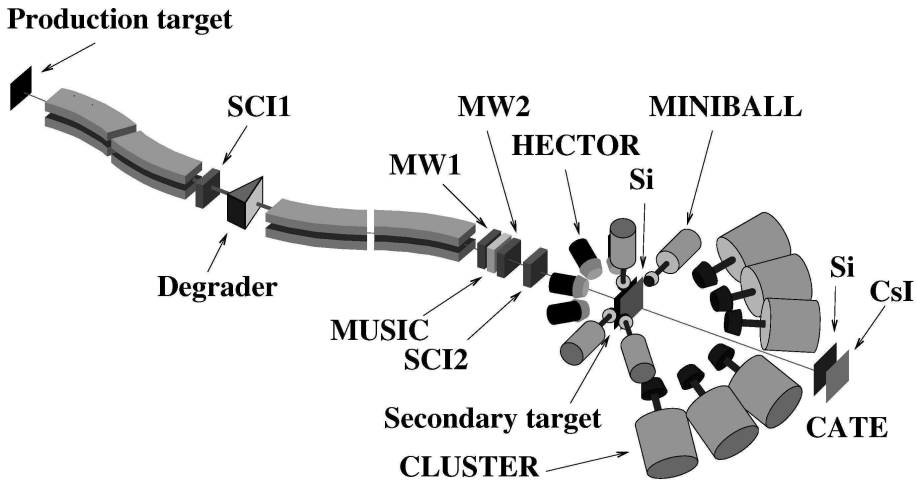

Fig. 1. Schematic layout of the RISING setup at the FRS. See text for details.

At the final focus of the FRS, a reaction target is placed. For Coulomb excitation experiments a ^{197}Au target of 0.4 to 2.0 g/cm^2 thickness is used, while two step fragmentation experiments are carried out with a 0.7 g/cm^2 ^{9}Be target. The reaction products are selected using the calorimeter telescope array CATE, consisting of 3×3 Si-CsI(Tl) modular ΔE-E telescopes 1400 mm downstream of the target.[10] The energy loss in the Si detectors provides a good charge resolution for unambiguous Z identification after the secondary target. Due to the parallel momentum distribution in fragmentation processes, the total energy measurement of the fragments is insufficient to completely distinguish masses. The position sensitive CATE Si detectors and a single equal type Si detector placed directly after the target serve as tracking detectors for a proper Doppler correction. In the case of Coulomb excitation, unwanted nuclear contributions can be excluded by selecting scattering angles corresponding to sufficiently large impact parameters for which the multiwire detectors MW1 and MW2 upstream the target are needed.

In order to measure γ-rays emitted by excited states, the target area is surrounded by numerous detectors:

(i) 15 Cluster Ge-detectors, positioned in three rings at extreme forward angles,
(ii) seven six-fold segmented MINIBALL triple Ge-detectors, arranged in two rings with central angles of 45° and 85°,
(iii) the HECTOR array, consisting of eight large volume BaF_2 detectors, situated at angles of 85° and 142°.

The fragmentation technique at relativistic beam energies allows for in-beam spectroscopy of β-unstable nuclei far from stability with very thick targets, partially counterbalancing the low beam intensities. However, the beam slows down in the secondary target, which consequently causes a velocity distribution of the projectile

at the time of photon emission, depending on the target thickness and the lifetime of the excited state. Accordingly, the spread in secondary beam velocity and the opening angle of the γ-detectors effect the γ-ray energy resolution after Doppler-correction.[1]

3. Mirror Symmetry in $A = 36$, $T = 2$ Nuclei

The new $N, Z = 14(16)$ shell stabilization and the $N = 20$ shell quenching in $^{32}\mathrm{Mg}_{20}$ are expected to be dominated by the monopole part of the two-body interaction. Moreover, the scenario is anticipated to be symmetric with respect to the isospin projection T_z and may not or little effected by neutron binding energy differences.[6,7] The ideal site in the Segré chart where this can be verified is the $N = 20$ mirror region along the light Ca ($Z = 20$) isotopes. The lightest Ca isotope with detailed spectroscopy is ^{38}Ca, while no excited states are known for the $N = 16$ isotope, thus the mirror nucleus of the doubly magic ^{36}S is of high interest.

Recently, the Coulomb energy difference of isobaric analog states and especially the mirror energy difference in $T_z = \pm T$ pairs of nuclei have been extensively studied.[11,12] In connection with precise large-scale shell model calculations they have proved to be a sensitive spectroscopic probe to investigate orbital radii in excited states and reduced overlap of identical proton and neutron orbitals at the driplines.[13] Experimental information can be deduced from the ΔE_M measurement between ^{36}Ca and ^{36}S.

The two step fragmentation technique of a stable ^{40}Ca and an intermediate ^{37}Ca beam was used to populate excited states in ^{36}Ca. In Fig. 2 Doppler corrected γ-ray spectra of ^{36}Ca are shown for the MINIBALL, Cluster and HECTOR detectors. The energy of the $2_1^+ \rightarrow 0^+$ transition has been determined to be 3015(16) keV from the two Ge-detector arrays, resulting in $\Delta E_M = -276(16)$ keV for the $A = 36$, $T = 2$ mirror pair. Surprisingly, this new value is significantly larger than mirror energy differences observed in the *sd* shell for $T = 1$ states and predominantly single-j $T = 1$ valence states in the *pf* shell.[14] Other known $T = 2$ mirrors in the *sd* shell, $A = 24$ and 32, also exhibit much smaller mirror energy differences of $-102(11)$ keV and $-117(12)$ keV, respectively.[15,16] A comparable mirror energy difference can be found in the *p* shell for the $A = 14$, $T = 1$ nuclei with $\Delta E_M = -422(10)$ keV for their $2_1^+ \rightarrow 0^+$ transition.[14] Though in general the $T = 2$ mirror energy differences are larger than the $T = 1$ values, which may be due to the proton-rich partner lying closer to the dripline, the unique $A = 36$ and $A = 14$ cases are obvious.

In a first systematic attempt based on the isospin symmetric interaction USD, mirror energy differences in the *sd* shell were calculated for astrophysical application to the *rp*-process, but do not reproduce the experimental value of the $A = 36$, $T = 2$ mirror pair by a large margin.[17,18] In a preliminary approach we have used the experimental single particle energies from the $A = 17$, $T = 1/2$ mirrors and applied on a modified USD interaction.[19] Monopole corrections were applied to reproduce the $Z, N = 14, 16$ shell gaps, the $I^\pi = 2_1^+$ excitation energies and the

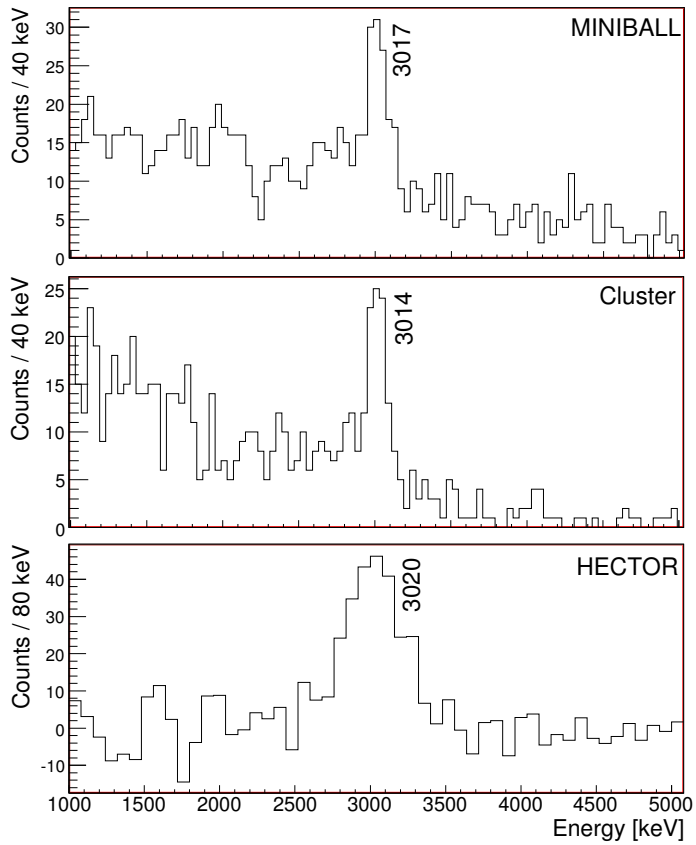

Fig. 2. Doppler corrected ^{36}Ca gated γ-ray spectra measured with the MINIBALL, Cluster and HECTOR detectors. For the HECTOR array the background was subtracted.

Table 1. Comparison of shell model calculation with experimental values for ^{36}Ca and ^{36}S.

	$E_{2_1^+}$ [keV]		π-gap [MeV]		ν-gap [MeV]	
Nucleus	Exp.[a]	SM[b]	Exp.	SM	Exp.	SM
^{36}Ca	3015(16)[c]	3290	4.55(30)		4.16(9)	3.999
^{36}S	3290.9(3)	3558	4.524(2)[d]	4.244	5.585	

[a]From Ref. 14.
[b]Shell model calculation, see text for details.
[c]This work.
[d]Coulomb Corrected.

^{40}Ca single hole energies. The results are shown in Table 1 for ^{36}Ca and ^{36}S and yield a value of $\Delta E_M = -268$ keV, in agreement with the experimental result. Isospin symmetry is preserved in the interaction two-body matrix elements but not in the single particle energies used, indicating that the experimental single

particle energies account empirically for the one-body part of Thomas-Ehrman and/or Coulomb effects.[20,21]

4. The Subshell Closure at $N = 32, 34$ — Coulomb Excitation of ^{54,56,58}Cr

The neutron-rich Cr isotopes are located at a key point on the pathway from the $N = 40$ subshell closure via a deformed region to spherical nuclei at $N = 28$. Experimentally, possible subshell closures may develop at $N = 32, 34$ in neutron rich Ca isotopes as indicated by a rise in the 2_1^+ energy of ^{52}Ca.[22] The Ti and Cr isotopes exhibit a maximum of those energies at $N = 32$, while the Ni isotopes show constant values.[14,23,24]

Besides the 2_1^+ energies, $B(E2; 2_1^+ \rightarrow 0^+)$ values provide crucial information to test the evolution of subshell structures. Three experiments were performed to measure the Coulomb excitation of ^{54}Cr, ^{56}Cr and ^{58}Cr, where the known

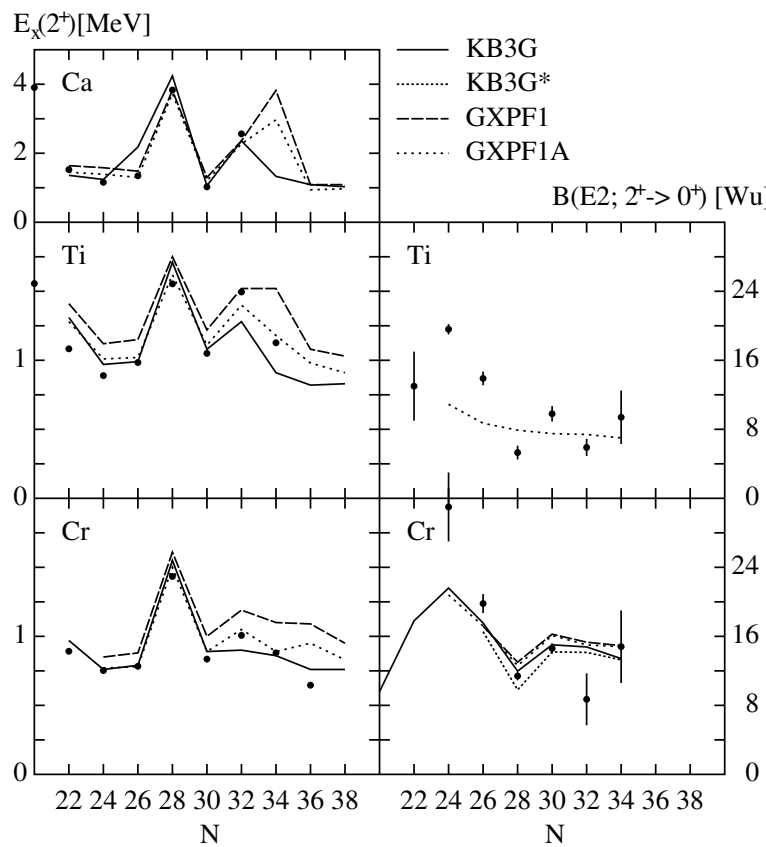

Fig. 3. Experimental $B(E2; 2_1^+ \rightarrow 0^+)$ values and 2_1^+ energies of neutron rich Ca, Ti and Cr isotopes in comparison to different shell model calculations.

$B(E2; 2_1^+ \rightarrow 0^+)$ value in ^{54}Cr served as normalization and reference for possible systematic errors in the analysis. Details of the experiment are given in the publication by A. Bürger *et al.*[25] The obtained Doppler corrected Cr spectra yield values of 8.7(3.0) W.u. for ^{56}Cr and 14.8(4.2) W.u. for ^{58}C. The results of this experiment are shown in Fig. 3 together with the experimental $B(E2; 2_1^+ \rightarrow 0^+)$ and 2_1^+ systematics of the Ti and Cr isotopes in comparison to various shell model calculations (KB3G, GXPF1, GXPF1A).[25,26–28]

The local peak in the $N = 32$ 2_1^+ energies is confirmed by a minimum of the $B(E2; 2_1^+ \rightarrow 0^+)$ values in the present experiment and a recent result for Ti isotopes.[26] For $N = 34$, however, the gap is developed in Cr and Ti which leaves ^{54,56}Ca as the crucial experimental probes. The shell model calculations reproduce the variation in the 2_1^+ energies. However, the $B(E2; 2_1^+ \rightarrow 0^+)$ values are virtually unchanged in the different approaches and almost constant from $N = 30$ to 34.

5. Triaxiality in ^{134}Ce and ^{136}Nd

As nuclear properties are investigated from closed shells toward the mid-shell regions, a transition from spherical to deformed shapes takes place in the mass $A \approx 130$ region. Since the origin of the deformation is mainly of quadrupole nature and the shape is connected with the collective motion of the nucleons, this influences the nature of low lying 2^+ states. The properties of these 2^+ states can be related to quadrupole triaxiality. However, the shape may not be well defined due to surface vibrations, resulting in a γ-soft configuration. To gain information on the nuclear shape of ^{134}Ce and ^{136}Nd, two nuclei which are candidates for being cores of chiral twin bands, relativistic Coulomb excitation experiments were performed. Here, not only the first 2_1^+ but also the second 2_2^+ state was observed for the first time after relativistic Coulomb excitation.

Detailed information on the experiment will be given in an upcoming paper.[29] The results of this experiment, given in Table 2 and Fig. 4, can be compared with a nuclear model, namely the asymmetric rotor model for a rigid triaxial nucleus.[30] The model can be extended to account for intrinsic vibrations of the nuclear surface, introducing an additional parameter μ which specifies the deformability of the surface in this soft asymmetric rotor model.[31] Details of this comparison are discussed by T. Saito *et al.*[29]

Table 2. $B(E2)$ values of ^{132}Ba, ^{134}Ce and ^{136}Nd depopulating the 2_1^+ and 2_2^+ states.

Transition	^{132}Ba $B(E2)$ [W.u.]	^{134}Ce $B(E2)$ [W.u.]	^{136}Nd $B(E2)$ [W.u.]
$2_1^+ \rightarrow 0^+$	42(4)[a]	52(5)[a]	80(11)
$2_2^+ \rightarrow 0^+$	3.9(4)[a]	≤ 11	11(3)
$2_2^+ \rightarrow 2_1^+$	144(14)[a]	≤ 140	182(93)

[a]From Ref. 14.

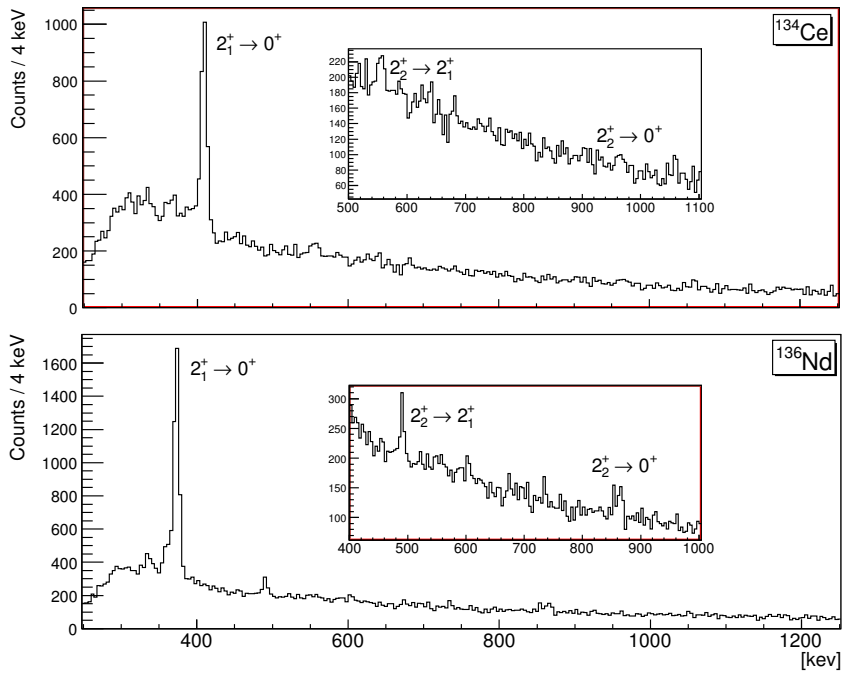

Fig. 4. Doppler corrected γ-ray spectra for ^{134}Ce and ^{136}Nd.

6. Summary

The shown results demonstrate the feasibility of high resolution γ-ray spectroscopy at relativistic energies utilizing the two-step fragmentation or Coulomb excitation technique with RISING. The ability of the SIS facility to accelerate all stable nuclei to several hundred MeV and the ensuing selection of fragmentation or fission products enables the study of interesting nuclear phenomena arising in regions far away from the valley of stability.

Acknowledgments

The collaboration would like to thank the EUROBALL Owners Comittee, the MINIBALL collaboration and the HECTOR collaboration for providing their γ-detectors to the RISING fast-beam campaign at GSI. This work was supported by the German BMBF under grant Nos. 06BN-109, 06K-167 and by the Polish State Committee for Scientific Research (KBN grant No. 620/E-77/SPB/GSI/P-03/DWM105/2004-2007).

References

1. H. J. Wollersheim *et al.*, *Nucl. Instr. Meth.* **A537** (2005) 637.
2. H. Geissel *et al.*, *Nucl. Instr. Meth.* **B70** (1992) 286.

3. J. Eberth *et al.*, *Nucl. Instr. Meth.* **A369** (1996) 135.
4. A. Maj *et al.*, *Nucl. Phys.* **A571** (1994) 185.
5. E. Caurier *et al.*, *Phys. Rev.***C60** (1994) 225.
6. T. Otsuka *et al.*, *Phys. Rev. Lett.* **87** (2001) 082502.
7. H. Grawe, *Act. Phys. Pol.* **B34** (2003) 2267.
8. C. M. Petrache *et al.*, *Phys. Rev.* **C61** (2000) 011305(R).
9. K. Starosta *et al.*, *Phys. Rev. Lett.* **86** (2001) 971.
10. R. Lozeva *et al.*, *Nucl. Instr. Meth.* **A562** (2005) 298.
11. S. M. Lenzi *et al.*, *Phys. Rev. Lett.* **87** (2002) 122501.
12. A. P. Zuker *et al.*, *Phys. Rev. Lett.* **87** (2002) 142502.
13. G. de Angelis *et al.*, *Eur. Phys. J.* **A12** (2001) 51.
14. ENSDF database, `http://www.nndc.bnl.gov/ensdf/`
15. S. Kanno *et al.*, *Prog. Theor. Phys.* (Kyoto), Suppl. **146** (2002) 575.
16. P. D. Cottle *et al.*, *Phys. Rev. Lett.* **88** (2002) 172502.
17. B. A. Brown and B. H. Wildenthal, *Ann. Rev. of Nucl. Part. Sci.* **38** (1988) 29.
18. H. Herndl *et al.*, *Phys. Rev.* **C52** (1995) 1078.
19. Y. Utsuno *et al.*, *Phys. Rev.* **C60** (1999) 054315.
20. R. G. Thomas, *Phys. Rev.* **88** (1952) 1109.
21. J. B. Ehrman, *Phys. Rev.* **81** (1951) 412.
22. A. Huck *et al.*, *Phys. Rev.* **C31** (1985) 2226.
23. S. N. Liddick *et al.*, *Phys. Rev. Lett.* **92** (2004) 072502.
24. P. F. Mantica *et al.*, *Phys. Rev.* **C67** (2003) 014311.
25. A. Bürger *et al.*, *Phys. Lett.* **B622** (2005) 29.
26. D. C. Dinca *et al.*, *Phys. Rev.* **C71** (2005) 041302.
27. E. Caurier *et al.*, *Eur. Phys. J.* **A15** (2002) 145.
28. M. Honma *et al.*, *Phys. Rev.* **C69** (2004) 034335.
29. T. Saito *et al.*, to be published.
30. A. S. Davydov and G. F. Filippov, *Nucl. Phys.* **8** (1958) 237.
31. A. S. Davydov and A. A. Chaban, *Nucl. Phys.* **20** (1960) 499.